The contrast between Atlantic and Pacific surface water fluxes

Philip M. Craig *

David Ferreira

John Methven

Department of Meteorology, University of Reading, Reading, Berkshire, UK

October 14, 2016

* *Corresponding author email address:*
p.m.craig@pgr.reading.ac.uk

Abstract

The Atlantic Ocean is known to have higher sea surface salinity than the Pacific Ocean at all latitudes. This is thought to be associated with the Atlantic Meridional Overturning Circulation and deep water formation in the high latitude North Atlantic - a phenomenon not present anywhere in the Pacific. This asymmetry may be a result of salt transport in the ocean or an asymmetry in the surface water flux (evaporation minus precipitation; $E-P$) with greater $E-P$ over the Atlantic than the Pacific. In this paper we focus on the surface water flux.

Seven estimates of the net freshwater flux ($E-P-R$ including runoff, R), calculated with different methods and a range of data sources (atmospheric and oceanic reanalyses, surface flux datasets, hydrographic sections), are compared. It is shown that $E-P-R$ over the Atlantic is consistently greater than $E-P-R$ over the Pacific by about 0.4 Sv (1 Sv $\equiv 10^6$ m^3 s^{-1}). The Atlantic/Pacific $E-P-R$ asymmetry is found at all latitudes between 30°S and 60°N. Further analysis with ERA-Interim combined with a runoff dataset demonstrates that the basin $E-P-R$ asymmetry is dominated by an evaporation asymmetry in the northern high-latitudes, but by a precipitation asymmetry everywhere south of 30°N. At the basin scale, the excess of precipitation over the Pacific compared to the Atlantic ($\sim$ 30°S - 60°N) dominates the asymmetry. Also it is shown that the asymmetry is present throughout the year and quite steady from year to year. Investigation of the interannual variability and trends suggest that the precipitation trends are not robust between datasets and are indistinguishable from variability. However, a positive trend in evaporation (comparable to other published estimates) is seen in ERA-Interim, consistent with sea surface temperature increases.

Key words: evaporation, precipitation, runoff, moisture flux, salinity, freshwater transport, Meridional Overturning Circulation

1 Introduction

The Atlantic Ocean is known to have higher sea surface salinity (SSS) than the Pacific Ocean at all latitudes. In the northern hemisphere, differences of up to 2 psu (practical salinity units) are present in the subtropical gyres (Gordon *et al.*, 2015) and at high latitudes, with the difference reduced to 1 psu in the southern hemisphere subtropical gyres (Fig. 1a). Salinity patterns are linked to the hydrological cycle (Schmitt, 2008) with regions of high SSS corresponding to regions of positive $E-P$ (evaporation minus precipitation) and regions of low SSS corresponding to regions of negative $E - P$ (Fig. 1b). Some authors have attemped to use SSS as a "rain gauge" for the ocean (Ren *et al.*, 2014) and others have investigated how SSS has changed with the intensification of the hydrological cycle in recent decades (Skliris *et al.*, 2014). Durack and Wijffels (2010) found that the contrast in SSS between the Atlantic and Pacific has increased from 1950-2008, consistent with an intensified hydrological cycle expected from global warming conditions (Held and Soden, 2006).

The high salinity in the high latitude North Atlantic is associated with deep water formation through deep convection in the Greenland and Labrador Seas and a deep Atlantic Meridional Overturning Circulation (AMOC) (Marshall and Schott, 1999). There is no such deep convection in the North Pacific as SSS is too low for sinking to occur (Warren, 1983) and the Meridonal Overturning Circulation there is wind-driven and confined to the upper ocean. Various reasons have been put forward to explain the asymmetry in MOC, such as differences in basin geometry (Schmitt *et al.*, 1989; Ferreira *et al.*, 2010; Nilsson *et al.*, 2013), the configuration of mountain ranges (Schmittner *et al.*, 2011; Sinha *et al.*, 2012), interbasin salt fluxes (Weijer *et al.*, 1999) and the existence of multiple equilibria of the MOC (Huisman *et al.*, 2009) – see also the review by Weaver *et al.* (1999). In nearly all published hypotheses not involving multiple equilibria, the net surface water flux (evaporation minus precipitation; $E - P$) is a key element, either as a cause or as a consequence of the MOC asymmetry. Indeed, it seems natural that the larger net evaporation ($E - P > 0$) in the Atlantic than in the Pacific (well noted in the literature, at least for high-latitudes) should be part of any theory for the MOC and SSS asymmetry between basins.

Warren (1983) pointed out that the Pacific has a lower evaporation rate compared to the Atlantic at high latitudes. He also investigated the effect of the line of zero wind stress curl on salt advection into the northern North Atlantic and Pacific, and suggested that the tilted Atlantic zero wind stress curl line allowed for more salt advection than in the Pacific from the high salinity subtropics. Using updated datasets, Emile-Geay *et al.* (2003) drew a similar conclusion. They further suggested that moisture transport associated with the Asian monsoon could contribute to the freshening of the subpolar North Pacific (no such transport exists over the subpolar North Atlantic) although no quantification of this effect was offered. Revisiting the idea of Warren (1983), Czaja (2009) found that the tilted zero wind stress curl line coincides with the line separating net evaporation from net precipitation ($E - P < 0$) in the Atlantic but not the Pacific. Higher subopolar salinity in the Atlantic can therefore be maintained more easily in the Atlantic than in the Pacific. Czaja (2009) also investigated the temporal behaviour of the North Atlantic and North Pacific jet streams, finding the North Atlantic to be more variable, a feature which is efficient at driving salt advection into the subpolar gyre.

The higher subpolar North Atlantic mean evaporation rate noted by Warren (1983), Emile-Geay *et al.* (2003) and Wills and Schneider (2015) was attributed to higher Atlantic sea surface temperatures (SSTs). The colder Pacific SSTs were explained by Warren (1983) to be a result of cold upwelling in the subpolar North Pacific. However, Czaja (2009) argued that the higher subpolar Atlantic evaporation is simply a positive feedback: the higher rate of evaporation is caused by higher SSTs which is a result of the enhanced northward ocean heat transport (Trenberth and Caron, 2001) by the AMOC. Wills and Schneider (2015) found that atmospheric transient eddies and stationary-eddy vertical motion are dominant terms in setting zonal variations in the surface water flux for subpolar North Atlantic and Pacific. Transient eddies freshen the subpolar North Pacific (while salinifying the subpolar North Atlantic) because the Pacific storm track covers a larger area. Stationary-eddy vertical motion freshens the subpolar North Pacific more than the subpolar North Atlantic due to poleward motion and surface stress associated with the Aleutian low and subtropical high. The arguments of Wills and Schneider (2015) are linked to the relative width of the subpolar basins highlighted by Schmitt *et al.* (1989): the Atlantic is narrower so a greater fraction of it is affected by dry air coming off the downstream continent, thus the area-averaged evaporation rate is stronger.

Many previous studies have focused on the $E - P$ asymmetry between the far northern regions of both oceans, although Rahmstorf (1996) focused on the positive Atlantic $E - P$ north of 30°S. It is unclear where $E-P$ is the critical quantity since the SSS asymmetry between the basins exists at all latitudes. In addition, discussion of the $E - P$ asymmetry has often been framed, implicitly or explicitly, as an asymmetry in evaporation, neglecting the possible roles for precipitation and runoff.

In this paper we aim to answer the following questions:

1. How robust is the Pacific/Atlantic $E - P - R$ asymmetry across datasets?
2. Is the Pacific/Atlantic asymmetry present at all latitudes?
3. Is the $E - P - R$ asymmetry mainly due to an asymmetry in evaporation, precipitation or runoff?
4. Can interannual variability of $E - P$ be attributed to interannual variability in evaporation or precipitation?

To address these questions, we will compare various published freshwater flux estimates obtained with a range of methods. Importantly, we will show that $E - P$ from ERA-Interim (estimated using vertically integrated atmospheric moisture flux divergence or the forecast model E and P fields) combined with an independent estimate of R agree well with other estimates from both oceanic and atmospheric data. This step gives us ground to further explore the ERA-Interim E and P fields separately and address questions 3 and 4 above.

The budget calculations (for the atmosphere and ocean) used to compute the net surface water flux ($E - P$) and net freshwater flux ($E - P - R$) are summarized in section 2. A brief description of the selected datasets is given in section 3. These estimates are compared in section 4. In section 5, annual means, seasonal cycles and interannual variability of the evaporation and precipitation from ERA-Interim are discussed in the Atlantic and Pacific Oceans. Conclusions will be drawn in section 6. Note that, for completeness, results for the Indian Ocean are also shown but that our discussion largely focuses on the Atlantic and Pacific basins.

2 Budget Framework

This section describes the methods used to calculate the surface water flux from atmospheric data (section 2.1) and the net freshwater flux from oceanic data (sections 2.2 and 2.3). It should be noted that, although similar in spirit, these calculations use completely different inputs (wind and specific humidity on one side, temperature and salinity on the other) and yet, as will be demonstrated in section 4, they give remarkably similar results.

2.1 Atmospheric moisture budget

In the atmosphere evaporation minus precipitation ($e - p$, where e and p are rates at grid points), can be related to the vertical integral of the mass continuity equation for water vapour (Berrisford *et al.*, 2011):

$$e - p = \frac{\partial\, TCWV}{\partial t} + \nabla \cdot \frac{1}{g} \int_0^1 \mathbf{u} q \frac{\partial \tilde{p}}{\partial \eta} \mathrm{d}\eta \tag{1}$$

where $TCWV = \frac{1}{g} \int_0^1 q \frac{\partial \tilde{p}}{\partial \eta} \mathrm{d}\eta$ is the total column water vapour, g is gravitational acceleration, $\mathbf{u}$ is the velocity vector, q is specific humidity and $\tilde{p}$ is pressure. The second term on the right-hand side of eq. (1) is the vertically integrated moisture flux divergence (denoted div$\mathbf{Q}$ hereafter, here written in terms of η the terrain-following hybrid pressure co-ordinate used in the ERA-Interim reanalysis where $\eta = 1$ represents the surface and $\eta = 0$ represents the top of the atmosphere). Ice and liquid water are neglected as their mass transports are small when compared to those of water vapour (Berrisford *et al.*, 2011).

Integrated over long timescales, div$\mathbf{Q}$ approximately balances $e - p$ (Trenberth *et al.*, 2011) since the tendency term (first term on the right-hand side of eq. (1)) is orders of magnitude smaller than div$\mathbf{Q}$ and $E - P$. The annual mean ERA-Interim (1979-2014) div$\mathbf{Q}$ over the global oceans is shown in Fig. 1(b). As expected, moisture flux divergence implying net evaporation is found in the subtropics and convergence implying net precipitation is found in the Intertropical Convergence Zone (ITCZ) and in mid- to high-latitudes. Note the clear correspondence between the $e - p$ and SSS patterns: the regions of positive (negative) $e - p$ in Fig.1(b) correspond approximately to regions of high (low) salinity in (a). The subtropical gyres occupy regions of high SSS and $e-p$ with the highest open ocean SSS found in the North Atlantic subtropical gyre (D'Addezio and Bingham, 2014). Salinity minima are found slightly to the north of the ITCZ ($e-p$ minima) in both the Atlantic and Pacific due to northwards Ekman transport of salt (Tchilibou *et al.*, 2015). The salinity minimum caused by the South Pacific Convergence Zone (SPCZ) is also offset from the $e-p$ minimum due to Ekman transport.

2.2 Mass transport in the ocean

The net freshwater flux ($E - P - R$) can be estimated by completely independent means from oceanographic data alone. Consider the integral of the the mass continuity equation for the ocean over a fixed volume V between latitudes ϕ_N and ϕ_S and from the western to eastern boundaries of an ocean basin:

$$\frac{\mathrm{d}M}{\mathrm{d}t} + \oiint_{\partial V} \rho\mathbf{u}\cdot\mathbf{n}\mathrm{d}A = 0 \qquad (2)$$

where $M = \iiint_V \rho \mathrm{d}V$, ∂V is the boundary of the volume and $\mathbf{n}$ is the outward-facing normal vector. Assuming steady state, eq. (2) can be rewritten as:

$$P - E + R = \iint_{\phi_N} \rho\mathbf{u}\cdot\tilde{\mathbf{n}}\,\mathrm{d}x\mathrm{d}z - \iint_{\phi_S} \rho\mathbf{u}\cdot\tilde{\mathbf{n}}\,\mathrm{d}x\mathrm{d}z \qquad (3)$$

where $\tilde{\mathbf{n}}$ is the northward-pointing normal vector. This simply states that the difference between the flux across two longitude-height sections is equal to the net (integrated) input of water at the ocean's surface between the sections, $P - E = \iint_{\text{surf}}(p - e)\mathrm{d}x\mathrm{d}y$ (e and p as in eq. (1)), plus runoff R into the ocean basin. The latter is effectively the integrated flux across the western and eastern boundaries.

2.3 Oceanographic method to estimate freshwater transport

The mass balance equation (3) allows the calculation of $P - E + R$ from the mass fluxes through two sections. This method can be applied precisely in a General Circulation Model where the velocity field is known with high accuracy. On hydrographic sections, however, temperature, salinity and other tracers are measured at a range of depths at locations along a ship's route, but velocities are not. Horizontal velocities are estimated from thermal wind balance and determination of a reference velocity. Uncertainties in this method are so large that a direct estimation of $E - P - R$ from the mass balance eq. (3) is impractical on hydrographic sections. The uncertainty in estimates of $E - P - R$ can be significantly reduced by combining the mass balance with the salinity balance (Wijffels, 2001; Ganachaud and Wunsch, 2003; Talley, 2008).

Integration of the salt budget over a fixed volume, assuming that any sources of salt are negligible (Wijffels *et al.*, 1992), gives:

$$\frac{\partial M_s}{\partial t} + \oiint_{\partial V} \rho s \mathbf{u} \cdot \mathbf{n} \,\mathrm{d}A = 0 \tag{4}$$

where the mass of salt $M_s = \iiint_V \rho s \mathrm{d}V$ with salinity s. In steady state, eq. (4) becomes

$$\iint_{\phi_N} \rho s \mathbf{u} \cdot \tilde{\mathbf{n}} \,\mathrm{d}x\mathrm{d}z - \iint_{\phi_S} \rho s \mathbf{u} \cdot \tilde{\mathbf{n}} \,\mathrm{d}x\mathrm{d}z = 0. \tag{5}$$

The mass and salt balances, eqs. (3) and (5), can be combined using a reference salinity s_0 to re-scale the salt budget:

$$P - E + R = \iint_{\phi_N} \left(1 - \frac{s}{s_0}\right) \rho \mathbf{u} \cdot \tilde{\mathbf{n}} \,\mathrm{d}x\mathrm{d}z - \iint_{\phi_S} \left(1 - \frac{s}{s_0}\right) \rho \mathbf{u} \cdot \tilde{\mathbf{n}} \,\mathrm{d}x\mathrm{d}z. \tag{6}$$

This equation uses two observed properties (temperature and salinity) from hydrographic sections. As pointed out by Ganachaud and Wunsch (2003), uncertainties associated with estimation of $P - E + R$ (eq. (6)) are about one order of magnitude lower than attempting to estimate the same quantity directly from (3). Note also that, in practice, the choice of s_0 has little impact on the freshwater transport estimates (Talley, 2008).

When using eq. (6), the northern section is often set at the Bering Strait and the expression is approximated assuming a uniform salinity s_{BS} across the strait, yielding:

$$P - E + R = T_{\mathrm{BS}} \left(1 - \frac{s_{\mathrm{BS}}}{s_0}\right) - \iint_{\phi_S} \left(1 - \frac{s}{s_0}\right) \rho \mathbf{u} \cdot \tilde{\mathbf{n}} \,\mathrm{d}x\mathrm{d}z \tag{7}$$

where T_{BS} is the net (northward) mass transport across the Bering Strait. Note that for a south section ϕ_S in the Pacific, T_{BS} is positive (i.e. northward/outward of the domain defined by the two sections), but is negative for in the Atlantic (i.e. inward flux into the domain). The first term on the right-hand side of eq. (7) is sometimes referred to as the Bering Strait "leakage".

Variants of eq. (6) (or eq. (7)) are found in the literature. Wijffels (2001) sets the reference salinity equal to the mean salinity along each section and works with the salinity anomalies about the mean salinity. Wijffels *et al.* (1992) do not use a reference salinity when combining the mass and salt budgets, but rather express the salinity in kg of salt per kg of water:

$$(P - E + R) = \iint_{\phi_N} (1-s)\rho \mathbf{u} \cdot \tilde{\mathbf{n}} \, \mathrm{d}x\mathrm{d}z - \iint_{\phi_S} (1-s)\rho \mathbf{u} \cdot \tilde{\mathbf{n}} \, \mathrm{d}x\mathrm{d}z \qquad (8)$$

defining a true freshwater transport *i.e.* the part of the ocean transport which is "fresh". However, eq. (8) is heavily weighted towards the mass balance since $s \sim 0.035 \ll 1$, and so this method has the same limitations as the pure mass balance eq. (3).

3 Datasets

We compare estimates of $E - P - R$ (*i.e.* positive into the atmosphere) from seven different datasets. We do not aim to be exhaustive in our choice, but rather to include a range of methods available for such computations at the global scale. Importantly, these estimates include methods relying nearly exclusively on atmospheric or oceanographic data, while other methods combine measurements from both fluids. Note that Wijffels *et al.* (1992) calculated the first global distribution of freshwater transport using the results of Baumgartner and Reichel (1975) for E, P and R in 5° latitude bands. However, this estimate produced a strongly negative value of $E - P - R$ for the Pacific. This was shown by Wijffels (2001) to be incorrect: it is likely the result of poor or sparse observations from Baumgartner and Reichel (1975). Estimates from Wijffels *et al.* (1992) will therefore not be discussed further.

3.1 Atmospheric reanalysis

We use monthly mean data from the ERA-Interim reanalysis dataset from the ECMWF (European Centre for Medium-Range Weather Forecasts) for the years 1979-2014 (Dee *et al.*, 2011). The data are on a full N128 Gaussian grid at $0.75° \times 0.75°$ horizonal resolution and with 60 vertical levels. ERA-Interim uses a 4D-VAR data assimilation scheme with 12-hourly analysis cycles which combine observations with prior information from the model. Pressure level parameters are provided every 6 hours and surface parameters are provided every 3 hours.

ERA-Interim allows for $E - P$ to be calculated in two ways: from div$\mathbf{Q}$ using eq. (1) and from separate evaporation and precipitation fields which are output as the accumulated (time-integrated) fluxes at the lower boundary over each forecast. In the reanalysis system the forecasts are restarted every 12 hours from the previous analysis. Many studies have used div$\mathbf{Q}$ to calculate $E - P$ (*e.g.* Seager and Henderson, 2013; Brown and Kummerow, 2014) but Berrisford *et al.* (2011) points out that the difference between div$\mathbf{Q}$ and $E-P$ from the forecast model is small when averaged globally so when $E - P$ is integrated over an ocean basin only a small difference should be expected between the div$\mathbf{Q}$ and forecast model calculations. Here, values of $E - P$ (div$\mathbf{Q}$) from ERA-Interim will be combined with run-off estimates R from Dai and Trenberth (2002) (see below).

Dai and Trenberth (2003) estimated freshwater transports using $P-E$ from ECMWF (1979-1993) and NCEP/NCAR (1979-1995) reanalyses along with improved estimates of R from Dai and Trenberth (2002). These improved estimates of R were calculated from streamflow data for the world's 921 largest rivers at the furthest downstream gauge station which were then extrapolated to the river mouth. By extrapolating to the river mouth total global runoff was increased by 19% compared to previous datasets. By using reanalysis $P - E$ and the new R dataset (along with the same transport of 0.794 Sv (1 Sv $\equiv 10^6\,\mathrm{m}^3\,\mathrm{s}^{-1}$) as used by Wijffels *et al.* (1992) at the Bering Strait), Dai and Trenberth (2003) showed that the southward freshwater transport at all latitudes in the Atlantic and northward transport in the South Pacific are stronger than shown by Wijffels *et al.* (1992).

3.2 Independent estimates of e and p

The oceanic freshwater budget was quantified by Schanze *et al.* (2010) using atmospheric data from independent sources for surface freshwater fluxes. GPCP (Global Precipitation Climatology Project, Adler *et al.*, 2003) was used for precipitation and OAFlux (Objectively Analyzed air-sea Fluxes; Yu and Weller, 2007) for evaporation for the period 1987-2006, with the Dai and Trenberth (2002) runoff. Freshwater transports were estimated by integrating $e - p - r$ meridionally over each basin. A transport of 0.8 Sv is used at the Bering Strait and iceberg forcings of 0.01 and 0.06 Sv are added near Greenland and Antarctica respectively. This method leaves an imbalance of 0.32 Sv at 55°S which could not be constrained to a particular basin.

3.3 Hydrographic sections

Ganachaud and Wunsch (2003) used geostrophic inverse box modeling on hydrographic sections from the World Ocean Circulation Experiment (WOCE) to estimate $E - P - R$ from ocean transports using eq. (6). The model used determines a high-resolution geostrophic velocity field to ensure that the circulation allows for near-conservation of mass, heat and salt. Four sections were used in both the Atlantic and Pacific and three used in the Indian Ocean. The Indonesian Througflow (ITF) transport was 15 ± 5 Sv from the 1989 JADE section (Ganachaud *et al.*, 2000). Note that using data from hydrographic sections has the effect of aliasing ocean variability as each section was recorded in a different month and/or a different year. For complete details of the routes and dates of each section see Fig. 1 in Ganachaud and Wunsch (2003).

Talley (2008) used absolute geostrophic velocity analyses from hydrographic sections by J. Reid, combined with Ekman transports using NCEP reanalysis winds to estimate freshwater transports using eq. (7). Geostrophic reference velocities were adjusted to ensure mass balance through each section. A reference salinity of $s_o = 34.9$ g/kg was used and the transports through the Bering Strait and the ITF were set to 1

Sv and 10 Sv respectively.

3.4 Ocean reanalysis

Valdivieso *et al.* (2014) computed freshwater transports from the University of Reading UR025.4 ocean reanalysis (1993-2010) at $1/4°$ resolution. This reanalysis uses a variational method with the NEMO ocean modelling framework to constrain the ocean state by numerous observations (AVISO, Argo, etc.). The simulation is forced by ERA-Interim atmospheric reanalysis at the ocean surface and the Dai and Trenberth (2002) runoff at the land mask edge. Note that the e field used to force the model is not taken from the ERA-Interim reanalysis, but recomputed as a function of the modeled SST. In addition, $E - P - R$ estimates from Valdivieso *et al.* (2014) include increments from the data assimilation method, *i.e.* it is assumed that assimilation increments to the ocean state, required by oceanic observations, represent errors in the surface forcing.

The "Estimating the Circulation and Climate of the Ocean" project version 4 (ECCOv4; Forget *et al.*, 2015) uses an adjoint-based method at $\sim 1°$ resolution with the MITgcm to fit the time-evolving (1992-2011) ocean state to numerous observations (WOCE sections, Argo, sea level anomalies, sea ice concentration, satellite SST products, etc). Freshwater transport divergences shown here are computed using eq. (3). Note that, as for the UR025.4 ocean reanalysis, atmospheric variables from ERA-Interim are used to compute air-sea fluxes (from bulk formulae and the simulated ocean state) and that they are adjusted as part of the optimization procedure to fit the modeled trajectory to ocean observations.

4 Comparison of $E - P - R$ estimates

In this section we compare the seven datasets described in section 3 and shown in Figs. 2 and 3. To recap, the estimates from ERA-Interim and Dai and Trenberth (2003) (ERA-40) combine atmospheric reanalyses with the Dai and Trenberth (2002) runoff estimate. Schanze *et al.* (2010) also uses atmospheric data, with E and P coming from separate datasets. Valdivieso *et al.* (2014) and ECCOV4 are both based on ocean reanalyses while Ganachaud and Wunsch (2003) and Talley (2008) use oceanographic observations alone.

Fig. 2 shows $E-P-R$ for the Atlantic, Pacific and Indian basins for each dataset described in section 3; panel (a) corresponds approximately to the latitudinal band 35°S-45°N and panel (b) to 35°S-65°N. The exact latitudinal boundaries used in calculating each estimate are shown in Table 1. Error bars are shown for most of the estimates although Dai and

Trenberth (2003) and Schanze *et al.* (2010) did not provide any estimates of uncertainty. The error bars on the ERA-Interim based estimated are a combination of interannual variability and the div$\mathbf{Q} - (E - P)$ residual using the error in quadrature method. The uncertainties presented by Ganachaud and Wunsch (2003) include uncertainties in the Ekman transport (set to 50% of the initial value) and model error which is dominated by aliasing of ocean variability (see section 3.3). Talley (2008) used a Monte Carlo approach to estimate the errors in the Ekman and geostrophic components of freshwater transports. For a full discussion of the error calculations performed, refer to section 2.3 of Talley (2008). The uncertainties presented for the ECCOv4 estimate represent interannual variability of the freshwater divergences. Valdivieso *et al.* (2014) presented uncertainties which represent interannual variability in the eddy and throughflow components of freshwater transport.

All estimates show that the Atlantic has a higher $E - P - R$ than the Pacific at both latitude ranges. Most of the estimates suggest that Indian $E - P - R$ is almost as high as the Atlantic in (a), with two suggesting that the Indian $E - P - R$ is greater. Most studies suggest that the Pacific has a low $E - P - R$ for the latitude range in (a) except for Schanze *et al.* (2010) who find a high $E-P-R$ value for the Pacific that is close to the Atlantic values. ERA-Interim matches ERA-40 (Dai and

Trenberth, 2003) in the Atlantic and Pacific and has higher $E - P - R$ in the Indian Ocean. The error bars are small, indicating that the budget residual and interannual variability of ERA-Interim $E - P$ is low and that the asymmetry between Atlantic and Pacific is steady in time. The larger error bars for the Pacific suggest that interannual variability of $E - P$ is higher or that the budget residual is higher (or a combination of both). The oceanographic estimates of Ganachaud and Wunsch (2003) and Talley (2008) match within their uncertainty estimates in all basins. The ECCOv4 estimate agrees remarkably well with the ERA-Interim estimate in all basins. Valdivieso *et al.* (2014), however, is consistently higher than all other estimates apart from Schanze *et al.* (2010) in the Pacific.

When extending the domain further north (Fig. 2b), the asymmetry between the Atlantic and Pacific oceans becomes stronger as three of the estimates indicate that the Pacific has negative $E - P - R$ while the Atlantic $E - P - R$ remains positive in all estimates. Talley (2008) actually finds that Atlantic $E - P - R$ *increases* with the northward extension of the domain (see below). Note that Valdivieso *et al.* (2014) gives lower $E - P - R$ than both atmospheric reanalyses and ECCOv4 possibly due to the more northerly extent used (see Table 1). Overall, the estimates are consistent in highlighting the differences in $E - P - R$ between ocean basins.

In order to see whether the differences between basins is found (and robust) at smaller scale, $E-P-R$ in latitude bands are shown in Fig. 3. The size of these bands is limited by the resolution of the Ganachaud and Wunsch (2003) and Talley (2008) estimates which are based on the routes taken by ships collecting the hydrographic sections. In the midlatitude North Atlantic, Talley (2008) produces a band with positive $E-P-R$ whereas the other estimates give negative values. This explains why the basin-integrated $E-P-R$ from Talley (2008) increases when the domain is extended to 60°N in Fig. 2(b). Inspection of $e-p$ (Fig. 1) shows net precipitation poleward of 45°N in all basins. This value for the North Atlantic from Talley (2008) is clearly an outlier although there is a large uncertainty for that band. ERA-Interim and Dai and Trenberth (2003) are well matched in the midlatitude North Atlantic but ERA-Interim $E-P-R$ is greater in the northern and southern subtropics with the opposite occurring in the tropics. ECCOv4 agrees well with ERA-Interim throughout the Atlantic but has notably lower $E-P-R$ in the southern hemisphere subtropics. The error bars on the ERA-Interim div$\mathbf{Q}$, however, are somewhat larger in these bands than in the northernmost band due to residuals which are an order of magnitude larger. It is also important to note that these estimates are all taken over different time periods so important events may have been missed out.

In the northern hemisphere subtropical Pacific (Fig. 3b) both atmospheric reanalyses (and NCEP, not shown) show weak positive $E-P-R$ while four of the other estimates are negative (ECCOv4 is indistinguishable from zero). The strongly positive Pacific $E-P-R$ (in comparison to other estimates) from Schanze *et al.* (2010) shown in Fig. 2 is mainly due to a tropical band which has $E-P-R=0$. The other estimates suggest that the tropical band has negative $E-P-R$ with the atmospheric reanalyses producing stronger negative $E-P-R$ than Ganachaud and Wunsch (2003) and Valdivieso *et al.* (2014). From 47°N to the Bering Strait each estimate agrees that the Pacific has negative $E-P-R$ although it is worth noting that the estimates based on atmospheric data give values of $E-P-R$ which are more negative than the oceanographic estimates.

In the Indian Ocean (Fig. 3c) the atmospheric reanalyses do not agree as closely as they do over the other ocean basins. This difference appears to occur over the southern part of the ocean and may be a direct result of the different bands used (Table 1) which may also contribute towards ERA-Interim having the highest $E-P-R$ overall in that band. The two atmospheric reanalysis products agree much closer in the other two bands but there is more disagreement between the estimates in these bands (despite falling within error bars). One reason for this may be that the oceanographic estimates based on hydrographic sections do not represent climatology and are therefore significantly biased by various factors affecting the freshwater transport such as ITCZ location and wind speed. The different values of the ITF transport used by Ganachaud and Wunsch (2003) and Talley (2008) may also be a factor in the large differences between these estimates. All estimates are in good agreement in the subtropics with a range of approximately $E - P - R = 0.15$ Sv.

A key outcome of the above analysis is that the net freshwater flux $E - P - R$ from ERA-Interim div$\mathbf{Q}$ combined with Dai and Trenberth (2002) runoff agrees well with other estimates, both at basin scale and in latitude bands. We use this as a basis for further analyzing the ERA-Interim fields.

5 ERA-Interim E and P

As shown in section 4, the globally averaged residual between div$\mathbf{Q}$ and $E - P$ from time-average surface accumulated forecasts is small in ERA-Interim. The 1979-2014 annual mean globally-averaged residual is 0.06 ± 0.3 mm/day which is an order of magnitude higher than the residual of 0.003 ± 0.3 mm/day calculated by Berrisford *et al.* (2011) for a shorter time period (1989-2008). Residuals at the scale of ocean basins (Table 2) are also small and on the same order of magnitude as the global average. Additionally, basin-averaged residuals for both oceans are only small percentages of basin-averaged E and P (less than 3%). In the Atlantic the residual does not affect the sign of $E - P - R$ estimates (cf error bars in Fig. 2) but since the Pacific basin-averaged $E - P$ is close to zero, the sign of the net $E - P - R$ is therefore rendered uncertain (Fig. 2).

Estimates of the partition of $E - P$ into separate evaporation and precipitation estimates over the global oceans are known to be 8-9% too large in ERA-interim (Berrisford *et al.*, 2011) and they are also overestimated in other reanalyses (Trenberth *et al.*, 2011). Brown and Kummerow (2014) point out that this problem is particularly marked in tropical regions although this has improved from ERA-40 (Dee *et al.*, 2011). They suggest that observations of near-surface specific humidity from ships and buoys have a dry bias which results in an overestimation of evaporation and therefore precipitation. In the extratropics, however, precipitation tends to be underestimated. For example, England and Wales precipitation in ERA-Interim is only 72% of the observed rainfall (de Leeuw *et al.*, 2015), with similar results found for other countries at the end of the North Atlantic storm track.

We will now use the separate E and P fields (instead of div$\mathbf{Q}$) to further analyze the Atlantic/Pacific asymmetry.

5.1 Annual mean latitude bands

Fig. 4 shows the net freshwater flux and its constituent parts split into 10° latitude bands from 30°S to 60°N. Here, the fluxes are area-weighted averaged in each band to allow for a more meaningful comparison between ocean basins (e.g. a band in the tropical Pacific has much larger area than a band in the tropical Atlantic). Area-averaged evaporation, precipitation and runoff are denoted by $\bar{e}$, $\bar{p}$ and $\bar{r}$ respectively.

From Fig. 4 it is clear that, within each basin, $\bar{p}$ is more variable than $\bar{e}$ across latitudinal bands, with peaks in the deep tropics showing the location of the ITCZ. Evaporation decreases with latitude in the northern hemisphere, reflecting the influence of SST on evaporation (D'Addezio and Bingham, 2014) as well as the lower relative humidity characteristic of the subtropical atmosphere (due to air coming from neighbouring continents and descending into the boundary layer in the subtropical highs). In the Atlantic (Fig. 4a), runoff has a particularly large impact on the net surface flux: despite $\bar{e}$ exceeding $\bar{p}$ in the 0°S-10°S band, the net flux is negative because of large runoff ($\bar{r}$) from rivers such as the Amazon and Congo.

To further localize the asymmetries seen at large scale (Figs. 2 and

3), the differences (Pacific minus Atlantic) are shown in Fig. 5. The most noticeable asymmetry is that Pacific $\bar{p}$ exceeds Atlantic $\bar{p}$ in almost all latitudes with the difference peaking slightly above 100 cm/yr in the 20-10°S band, likely due to the presence of the SPCZ. Note that south of 30°N $\bar{e}$ is remarkably similar in both ocean basins.

In the 50°N-60°N band, Atlantic $\bar{p}$ is 15 cm/yr greater than in the Pacific. Note that this result is sensitive to the choice of the latitudinal extents: for slightly larger bands (Emile-Geay *et al.*, 2003; Wills and Schneider, 2015), $\bar{p}$ is similar across basins and $\bar{e}$ is greater in the Atlantic than the Pacific. Polewards of 40°N the Atlantic $\bar{e}$ exceeds the Pacific $\bar{e}$ by about 20 cm/yr: this is likely related to higher SSTs in the North Atlantic than the North Pacific (Warren, 1983) and the greater fraction of the North Atlantic affected by the advection of cold, dry air from the continents (Schmitt *et al.*, 1989). Wills and Schneider (2015) argued that the asymmetry in the subpolar regions is primarily due to moisture fluxes from transient eddies which cause negative $E-P$ over the subpolar North Pacific and positive $E-P$ over the subpolar North Atlantic. The total runoff into the Atlantic is greater than into the Pacific with most of the difference between the two basins occurring in the 0°-10°N and 10°S-0° bands where some of the world's largest rivers can be found. The mouths of the two largest (Amazon and Congo) plus three of the top twenty are in the band to the south of the equator (Dai and Trenberth, 2002). The Orinoco (third largest) and three more of the top forty discharge into the Atlantic band immediately north of the equator.

Although a larger $\bar{e}$ is found in the North Atlantic than in the North Pacific, the asymmetry in the net freshwater flux across the basins is mostly caused by an asymmetry in $\bar{p}$, *i.e.* relatively stronger precipitation in the Pacific. There are only three 10° bands where Pacific $\bar{e} - \bar{p} - \bar{r}$ is greater. Two of which (10°S-0° and 0°-10°N) are a result of the strong asymmetry in $\bar{r}$ (masking a large precipitation excess in the Pacific) and the other is the narrow northern most band in the Pacific which contributes very little to the basin-averaged net flux. Note that despite the fact that these bands have less negative $\bar{e} - \bar{p} - \bar{r}$ in the Pacific, the salinity asymmetry still holds at all latitudes.

5.2 Seasonal variation

Fig. 6 shows the seasonal cycle of $\bar{e}$ and $\bar{p}$ for each ocean basin; the maps of the climatological seasonal means of $e - p$, e and p are shown in Figs. 7-9. Atlantic and Pacific mean evaporation rates are very similar (and quite constant at $\sim$4 mm/day). There is however a substantially lower precipitation rate in the Atlantic than in the Pacific, with Atlantic $\bar{p}$ near 2.5 mm/day compared to 4 mm/day in the Pacific. These features are present throughout the year, with the $\bar{e} - \bar{p}$ always positive over the Atlantic and always close to zero over the Pacific. In the Pacific, $\bar{e}$ and $\bar{p}$ have similar annual cycles with a decrease from January to May followed by an increase during the rest of the year. The annual cycle of $\bar{e}$ has a similar amplitude (~ 0.7 mm/day) in both basins but the amplitude of $\bar{p}$ is weaker in the Pacific (~ 0.5 mm/day compared to ~ 0.8 mm/day).

These effects are also reflected in the spatial pattern of seasonal $e-p$ which largely follows the spatial pattern of precipitation (Figs. 7-9). The subtropical regions (where $e - p > 0$) are characterized by a lack of precipitation in all seasons with the shape and size of the region of positive $e - p$ approximately matching the shape and size of the regions with $p <$ 2 mm/day. Seasonal variations of evaporation (Fig. 8) are most noticeable in the subtropical maxima and in the peaks over western boundary currents. Both oceans show maxima of evaporation in the northern hemisphere winter which is a result of increased wind speeds and the lower relative humidity. The advection of dry (subsaturated) winter air from continents to the oceans maintains high rate of evaporation, and therefore high wintertime latent heat flux, over the western part of basins, and notably over Western Boundary Currents such as the Gulf Stream and Kuroshio (Yu and Weller, 2007).

Further decomposing the seasonal cycle into latitudinal bands shows that the October/November peak in Atlantic $\bar{p}$ occurs in the northern hemisphere (Fig. 10b). During autumn the water vapour content of the subtropics is higher due to increased evaporation (Fig. 8d) and this is picked up by the storm tracks leading to increased meridional water vapour transport. D'Addezio and Bingham (2014) also attribute the autumn peak in subtropical North Atlantic precipitation to African easterly wave activity and tropical storm activity. Wang *et al.* (2013) highlights the influence of seasonal cycle of SSTs and the Atlantic Warm Pool (AWP) area, both of which peak in September along with $\bar{p}$ in the 15°N-35°N band (the AWP is a region of SST $>$ 28.5°C in the western tropical North Atlantic, 5°N-30°N). A minimum of SSS also occurs in the AWP region in September with a maximum in March when the AWP disappears (a month after the $E - P$ maximum). Initially the peak is in the subtropics but is later maintained at higher latitudes in winter (Figs. 9a,d). The double peak in tropical Atlantic precipitation is a due to the seasonal migration of the ITCZ which dominates the tropical SSS seasonal cycle (Boyer and Levitus, 2002).

The annual cycle of Pacific $\bar{p}$ (Fig. 11(b)) is also dominated by the northern hemisphere (reflecting the fact that most of the domain used to define the Pacific in this study is in the northern hemisphere), with the May-July minimum occuring in the midlatitudes due to a relatively weak storm track. The peaks in $\bar{p}$ in the northern subtropics in August and during winter in the midlatitudes are due to the same process found in the subtropical North Atlantic at the same times of year.

5.3 Interannual variability

The interannual variability of evaporation, precipitation, $\bar{e} - \bar{p}$ and div$\mathbf{Q}$ are shown along with the GPCP estimate of precipitation (Adler *et al.*, 2003) as anomalies from their respective annual means in Fig. 12. Precipitation time series are shown as $-\bar{p}$ in order to simplify the comparison with $\bar{e} - \bar{p}$ and div$\mathbf{Q}$. Until 2002, ERA-Interim precipitation appears to match GPCP variability well (particularly over the Atlantic) but the two datasets differ significantly in 2002-06. This is particularly evident over the Pacific where ERA-Interim $-\bar{p}$ increases sharply while $-$GPCP does not. This shift in precipitation is due to a problem with the assimilation of rain-affected radiances that caused an incorrect drying of the atmosphere (Dee *et al.*, 2011). Note the large offset between div$\mathbf{Q}$ and $\bar{e} - \bar{p}$ in the Pacific (Fig. 12b). ERA-Interim does, however, capture some of the El Niño-driven variability *i.e.* the 1997-98 El Niño is shown by a dip in $-\bar{p}$ by both ERA-Interim and GPCP. The Atlantic appears to be less affected by the assimilation problems: the GPCP variability from 2004-06 is reproduced in $-\bar{p}$ while still offset from $-$GPCP by $\sim$ 3 cm/yr. ERA-Interim also successfully reproduces the large $-\bar{p}$ decrease (a subsequent decrease in $\bar{e}-\bar{p}$) in 2010 associated with a record low North Atlantic Oscillation (NAO) Index and a 30% reduction in the AMOC (Roberts *et al.*, 2013; Bryden *et al.*, 2014). Increases in the area of the AWP on interannual timescales are shown to reduce $E - P$ due to increased SSTs and therefore increased moisture convergence into the region resulting in increased precipitation (Wang *et al.*, 2013). This then causes negative SSS anomalies which Wang *et al.* (2013) speculated may have an impact on the strength of the AMOC.

Evaporation appears to be less variable than precipitation in both basins and contributes less to the variability of ERA-Interim $\bar{e} - \bar{p}$. In the Pacific, however, evaporation changes contribute significantly to $\bar{e} - \bar{p}$ changes during the events such as the 1997-98 El Niño. This El Niño event is known to have caused an SSS decrease in the western equatorial Pacific and an SSS increase around the SPCZ, with precipitation considered to be one of the main mechanisms responsible for these SSS changes (Singh *et al.*, 2011). Increasing trends in $\bar{e}$ are evident in both basins throughout the ERA-Interim period. The Pacific trend is stronger than the Atlantic trend, with $\bar{e}$ increasing at a rate of 3.4 mm/yr/yr (least-squares linear fit) compared to 2.0 mm/yr/yr in the Atlantic. Increasing trends in oceanic evaporation are also present in other datasets (Iwasaki *et al.*, 2014; Su and Feng, 2015). Yu and Weller (2007) show that latent heat flux has increased in line with SSTs, resulting in an increase in evaporation rate of approximately 10 cm/yr from 1986-2005. This value compares well with ERA-Interim (Fig. 12) for the same period over the Pacific. As well as increasing SSTs, increasing wind speed has also been noted to contribute to increasing evaporation rates (Yu, 2007; Iwasaki *et al.*, 2014). Column-integrated water vapour has also been increasing as shown by the Special Sensor Microwave Imager (SSM/I), a trend which is well represented by reanalyses (Zhang *et al.*, 2013). Such an increase in column-integrated water vapour would require a corresponding increase in oceanic evaporation. This suggests that, unlike the precipitation trends, evaporation trends in ERA-Interim may be real and capture a physical change (although Brown and Kummerow (2014) show that ERA-Interim overestimates tropical evaporation).

Table 3 shows the correlations of $\bar{e}$, $-\bar{p}$, $\bar{e} - \bar{p}$ with div$\mathbf{Q}$ and the standard deviations of each field. The correlations highlight the inconsistencies between the two methods of calculating the surface water flux. The moisture flux divergence is better correlated with $\bar{e} - \bar{p}$ over the Atlantic than the Pacific. In particular, $-\bar{p}$ and div$\mathbf{Q}$ are poorly correlated over the Pacific, as expected from Fig. 12b. The standard deviations show that all Pacific fluxes are more variable than the Atlantic fluxes, with $-\bar{p}$

showing more interannual variablity than $\bar{e}$ over each ocean. Table 3 also shows that the asymmetry in $\bar{p}$ discussed in section 5.2 is also steady on interannual time scales, with Pacific $\bar{p}$ exceeding Atlantic $\bar{p}$ by approximately 40 cm/yr (not shown).

Although Fig. 12 also shows that $\bar{e} - \bar{p}$ mainly follows the interannual variability of $-\bar{p}$, the variability and trends in ERA-Interim are, as discussed above, not robust. That said, in the Atlantic before 2002 when ERA-Interim $\bar{p}$ matches GPCP well (correlation coefficient of 0.82), $-\bar{p}$ correlates with div$\mathbf{Q}$ better than with $\bar{e}$ (0.59 with $-\bar{p}$ over both oceans and 0.11 and 0.32 for $\bar{e}$ in the Atlantic and Pacific respectively). This suggests that $\bar{p}$ may well dominate $\bar{e} - \bar{p}$ variability in the Atlantic (at least before 2002). In the Pacific, correlation between ERA-Interim and GPCP before 2002 are poorer (only 0.43), and the dominant factor in variability cannot be deduced.

6 Summary and Conclusions

In this paper, we compare seven estimates of the net freshwater flux ($E - P - R$) over oceans, with a focus on the $E - P - R$ asymmetry between the Atlantic and Pacific oceans. Using ERA-Interim, which compares favourably with other estimates, we proceed on exploring the Atlantic/Pacific asymmetry on spatial (10° latitudinal bands) and temporal (seasonal, interannual) scales not accessible with some other datasets as well as investigating the role of precipitation, evaporation and runoff separately on the $E-P-R$ asymmetry. Our key findings are:

1. Net surface water fluxes estimated from atmospheric reanalyses are consistent with the ocean temperature and salinity observations used to estimate net freshwater fluxes from hydrographic section data. Both are also consistent with other datasets including recent ocean reanalyses. All estimates show that the Atlantic has greater positive $E-P-R$ than the Pacific. Pacific $E-P-R$ is approximately 0 Sv when the subpolar region is included and is approximately 0.4 Sv less than Atlantic $E-P-R$. Agreement between datasets is less strong in smaller latitude bands, however the $E-P-R$ still holds in the tropics and northern hemisphere although not in the southern hemisphere subtropics (due to the larger area of the Pacific).

2. We also find that ERA-Interim div$\mathbf{Q}$ and $E-P$ from surface forecast accumulations agree well when averaged globally or across ocean basins (consistent with Berrisford *et al.*, 2011) which establishes the validity of the ERA-Interim estimates for further diagnostics. Annual mean area-averaged evaporation, precipitation, runoff and $E-P-R$

across 10° latitude bands show that the asymmetry in $E - P - R$ in the high latitude northern hemisphere is mainly due to greater evaporation from the Atlantic (*e.g.* Warren, 1983; Emile-Geay *et al.*, 2003) but everywhere further south it appears that a stronger asymmetry in precipitation is more important in contributing to the asymmetry in $E - P - R$. At basin scale the $E - P - R$ asymmetry is largely caused by a precipitation asymmetry, rather than an evaporation asymmetry. One potential mechanism for this is linked to the patterns of stationary eddies over the two basins: the subtropical highs (areas of dry, descending air and low precipitation) cover a larger fraction of the Atlantic than the Pacific where ascendinding air (which leads to precipitation) covers a larger fraction of the basin. (Wills and Schneider, 2015).

3. The seasonal cycles of basin-averaged evaporation and precipitation show that the Atlantic/Pacific asymmetry exists throughout the year and is quite steady *i.e.* no particular season contributes to the asymmetry. Throughout the year, Pacific evaporation and precipitation are approximately equal but Atlantic precipitation is always less than evaporation. There is little difference between basin-averaged evaporation but basin-averaged precipitation is less in the Atlantic than

the Pacific for all months.

4. Because of problems with the assimilation of satellite data described by Dee *et al.* (2011), trends and interannual variability in precipitation are not robust (a conclusion supported by a comparison with GPCP precipitation). It is therefore problematic to explore the interannual variability of precipitation and its correlation with $E - P$. An upward trend in evaporation over recent decades in both basins appears to be consistent with the estimate from OAFlux. The interannual variability of the basin-averaged $E - P$ fluxes exhibit correlations with events such as large El Niño and NAO events.

Overall, a key finding of this study is that the $E-P-R$ asymmetry between the Atlantic and Pacific oceans exists at all latitudes, not just high-latitudes and that, outside of the high latitude northern hemisphere, an asymmetry in precipitation, rather than evaporation, has more influence on the asymmetry in $E-P-R$. Precipitation is largely driven by internal atmospheric processes (circulation patterns, atmospheric physics). This suggests that $E-P-R$ and possibly SSS and MOC asymmetries are caused by differences in atmospheric processes over the two basins. Some potential mechanisms have been suggested in the literature: the basin geometry (Schmitt *et al.*, 1989; Ferreira *et al.*, 2010; Nilsson *et al.*, 2013), the effect of mountain ranges (Schmittner *et al.*, 2011; Sinha *et al.*, 2012), variability and tilt of the Atlantic storm track (Czaja, 2009) and the patterns of stationary eddies (Wills and Schneider, 2015).

Considering on one hand the link between the high salinity of the Atlantic, the deep convection and the AMOC, and on the other the link between SSS distribution and $e-p-r$ pattern, we argue that any theory for the localization of the MOC in the Atlantic should provide an explanation for the $E-P-R$ asymmetry, and thus for the deficit of precipitation over the Atlantic. It is worth emphasizing that an $E-P-R$ asymmetry may not be neccessary to localize deep water formation in the Atlantic and favour an AMOC. This is notably the case in the presence of multiple equilibria of the MOC where localization is possible with no asymmetry or reversed asymmetry (smaller $E-P-R$ in the sinking basin, see Huisman *et al.* 2009). However, even if the real ocean is in this dynamical regime, the observed $E-P-R$ asymmetry provides a significant reinforcement of the AMOC (an atmospheric feedback or perhaps just a coincidence *e.g.* due to geometrical factors), and should be accounted for.

Acknowledgements

The lead author receives PhD studentship funding from the Natural Environment Research Council as part of the SCENARIO Doctoral Training Partnership (NE/L002566/1).

References

Adler, R., Huffman, G., Chang, A., Ferraro, R., Xie, P., and co-authors. 2003. The version-2 global precipitation climatology project (GPCP) monthly precipitation project analysis (1979-present). *J. Hydrometeor.*, **4**, 1147–1167.

Baumgartner, A. and Reichel, E. 1975. *The World Water Balance*. Elsevier.

Berrisford, P., Kållberg, P., Kobayashi, S., Dee, D., Uppala, S., and co-authors. 2011. Atmospheric conservation properties in ERA-Interim. *Quart. J. Roy. Meteor. Soc.*, **137**, 1381–1399.

Boyer, T. and Levitus, S. 2002. Harmonic analysis of climatological sea surface salinity. *J. Geophys. Res.Oceans*, **107**. 8006.

Brown, P. and Kummerow, C. 2014. An Assessment of Atmospheric Water Budget Components over Tropical Oceans. *J. Climate*, **27**, 2054–2071.

Bryden, H., King, B., McCarthy, G., and McDonagh, E. 2014. Impact of a 30% reduction in Atlantic meridional overturning circulation during 2009-2010. *Ocean Sci.*, **10**, 683–691.

Czaja, A. 2009. Atmospheric Control on the Thermohaline Circulation. *J. Climate*, **39**, 234–247.

D'Addezio, J. and Bingham, F. 2014. A subtropical North Atlantic regional atmospheric moisture budget. *J. Geophys. Res.Oceans*, **119**(12), 8731–8748.

Dai, A. and Trenberth, K. 2002. Estimates of Freshwater Discharge from Continents: Latitudinal and Seasonal Variations. *J. Hydrometeor.*, **3**, 660–687.

Dai, A. and Trenberth, K. 2003. New Estimates of Continental Discharge and Oceanic Freshwater Transport. In *AMS Symposium on Observing and Understanding the Variability of Water in Weather and Climate*, Long Beach, CA.

de Leeuw, J., Methven, J., and Blackburn, M. 2015. Evaluation of ERA-

Interim reanalysis precipitation products using England and Wales observations. *Quart. J. Roy. Meteor. Soc.*, **141**, 798–806.

Dee, D., Uppala, S., Simmons, A., Berrisford, P., Poli, P., and co-authors. 2011. The ERA-Interim Reanalysis: configuration and performance of the data assimilation system. *Quart. J. Roy. Meteor. Soc.*, **137**, 553–597.

Durack, P. and Wijffels, S. 2010. Fifty-Year Trends in Global Ocean Salinities and Their Relationship to Broad-Scale Warming. *J. Climate*, **23**, 4342–4362.

Emile-Geay, J., Cane, M., Naik, N., Seager, R., Clement, A., and van Geen, A. 2003. Warren revisited: Atmospheric freshwater fluxes and “Why is no deep water formed in the North Pacific”. *J. Geophys. Res.-Oceans*, **108**. 3178.

Ferreira, D., Marshall, J., and Campin, J.-M. 2010. Localization of Deep Water Formation: Role of Atmospheric Moisture Transport and Geometrical Constraints on Ocean Circulation. *J. Climate*, **23**, 1456–1476.

Forget, G., Campin, J.-M., Heimbach, P., Hill, C., Ponte, R., and Wunsch, C. 2015. ECCO version 4: an integrated framework for non-linear inverse modeling and global ocean state estimation. *Geosci. Model Dev.*, **8**(10), 3071–3104.

Ganachaud, A. and Wunsch, C. 2003. Large-Scale Ocean Heat and Freshwater Transports during the World Ocean Circulation Experiment. *J. Climate*, **16**, 696–705.

Ganachaud, A., Wunsch, C., Marotzke, J., and Toole, J. 2000. Meridional overturning and large-scale circulation of the Indian Ocean. *J. Geophys. Res.Oceans*, **105**(C11), 26117–26134.

Gordon, A., Giulivi, C., Busecke, J., and Bingham, F. 2015. Differences Among Subtropical Surface Salinity Patterns. *Oceanography*, **28**, 32–39.

Held, I. and Soden, B. 2006. Robust Responses of the Hydrological Cycle to Global Warming. *J. Climate*, **19**, 5686–1560.

Huisman, S., Dijkstra, H., von der Heydt, A., and de Ruijter, W. 2009. Robustness of multiple equilibria in the global ocean circulation. *Geophys. Res. Lett.*, **36**(1). L01610.

Iwasaki, S., Kubota, M., and Watabe, T. 2014. Assessment of various global freshwater flux products for the global ice-free oceans. *Remote Sens. Environ.*, **140**, 549–561.

Marshall, J. and Schott, F. 1999. Open-ocean convection: Observations, theory and models. *Rev. Geophys.*, **37**, 1–64.

Nilsson, J., Langen, P., Ferreira, D., and Marshall, J. 2013. Ocean Basin Geometry and the Salinification of the Atlantic Ocean. *J. Climate*, **26**, 6163–6184.

Rahmstorf, S. 1996. On the freshwater forcing and transport of the Atlantic thermohaline circulation. *Climate Dyn.*, **12**, 799–811.

Ren, L., Hackert, E., Arkin, P., and Busalacchi, A. 2014. Estimating the global oceanic net freshwater flux from Argo and comparing it with satellite-bases freshwater flux products. *J. Geophys. Res.Oceans*, **119**, 7869–7881.

Roberts, C., Waters, J., Peterson, K., Palmer, M., McCarthy, G., and co-authors. 2013. Atmosphere drives recent interannual variability of the Atlantic meridional overturning circulation at 26.5°N. *Geophys. Res. Lett.*, **40**(19), 5164–5170.

Schanze, J., Schmitt, R., and Yu, L. 2010. The global oceanic freshwater cycle: A state-of-the-art quantification. *J. Mar. Res.*, **68**, 569–595.

Schmitt, R. 2008. Salinity and the Global Water Cycle. *Oceanography*, **21**, 12–19.

Schmitt, R., Bogden, P., and Dorman, C. 1989. Evaporation Minus Precipitation and Density Fluxes for the North Atlantic. *J. Phys. Oceanogr.*, **19**, 1208–1221.

Schmittner, A., Silva, T., Fraedrich, K., Kirk, E., and Lunkeit, E. 2011. Effects of Mountains and Ice Sheets on Global Ocean Circulation. *J. Climate*, **24**, 2814–2829.

Seager, R. and Henderson, N. 2013. Diagnostic Computation of Moisture Budgets in the ERA-Interim Reanalysis with Reference to Analysis of CMIP-Archived Atmospheric Model Data. *J. Climate*, **26**, 7876–7901.

Singh, A., Delcroix, T., and Cravatte, S. 2011. Contrasting the flavors of El Niño-Southern Oscillation using sea surface salinity observations. *J. Geophys. Res.Oceans*, **116**(C6).

Sinha, B., Blaker, A., Hirschi, J.-M., Bonham, S., Brand, M., and co-authors. 2012. Mountain ranges favour vigorous Atlantic meridional overturning. *Geophys. Res. Lett.*, **39**. L02705.

Skliris, N., Marsh, R., Josey, S., Good, S., Liu, C., and Allan, R. 2014. Salinity changes in the World Ocean since 1950 in relation to changing surface freshwater fluxes. *Climate Dyn.*, **43**, 709–736.

Su, T. and Feng, G. 2015. Spatial-temporal variation characteristics of global evaporation revealed by eight reanalyses. *Sci. China Ser. D*, **58**, 255–269.

Talley, L. 2008. Freshwater transport estimates and the global overturning circulation: Shallow, deep and throughflow components. *Prog. Oceanogr.*, **78**, 257–303.

Tchilibou, M., Delcroix, T., Alory, G., Arnault, S., and Reverdin, G. 2015. Variations of the tropical Atlantic and Pacific SSS minimum zones and their relations to the ITCZ and SPCZ rain bands (1979-2009). *J. Geophys. Res.Oceans*, **120**, 5090–5100.

Trenberth, K. and Caron, J. 2001. Estimates of Meridional Atmosphere and Ocean Heat Transports. *J. Climate*, **14**, 3433–3443.

Trenberth, K., Fasullo, J., and Mackaro, J. 2011. Atmospheric Moisture Transports from Ocean to Land and Global Energy Flows in Reanalyses. *J. Climate*, **24**, 4907–4924.

Valdivieso, M., Haines, K., Zuo, H., and Lea, D. 2014. Freshwater and heat transports from global ocean synthesis. *J. Geophys. Res.*, **119**, 394–409.

Wang, C., Zhang, L., and Lee, S.-K. 2013. Response of Freshwater Flux and Sea Surface Salinity to Variability of the Atlantic Warm Pool. *J. Climate*, **26**, 1249–1267.

Warren, B. 1983. Why is no deep water formed in the North Pacific? *J. Mar. Res.*, **41**, 327–347.

Weaver, A., Bitz, C., Fanning, A., and Holland, M. 1999. Thermohaline Circulation: High-Latitude Phenomena and the Difference Between the Pacific and Atlantic. *Annu. Rev. Earth Pl. Sc.*, **27**, 231–285.

Weijer, W., de Ruijter, W., Dijkstra, H., and van Leeuwen, P. 1999. Impact of Interbasin Exchange on the Atlantic Overturning Circulation. *J. Phys. Oceanogr.*, **29**, 2266–2284.

Wijffels, S. 2001. Ocean Transport of Fresh Water. In G. Siedler, J. Church, and J. Gould, editors, *Ocean Circulation and Climate*, pages 475–488. Academic Press, London.

Wijffels, S., Schmitt, R., Bryden, H., and Stigebrandt, A. 1992. Transport of Freshwater by the Oceans. *J. Phys. Oceanogr.*, **22**, 155–162.

Wills, R. and Schneider, T. 2015. Stationary eddies and the zonal asymmetry of net precipitation and ocean freshwater forcing. *J. Climate*, **28**, 5115–5133.

Yu, L. 2007. Global Variations in Oceanic Evaporation (1958-2005): The Role of the Changing Wind Speed. *J. Climate*, **20**, 5376–5390.

Yu, L. and Weller, R. 2007. Objectively Analyzed Air-Sea Heat Fluxes for the Global Ice-Free Oceans (1981-2005). *Bull. Amer. Meteor. Soc.*, **88**, 527–539.

Zhang, L., Wu, L., and Gan, B. 2013. Modes and Mechanisms of Global Water Vapor Variability over the Twentieth Century. *J. Climate*, **26**, 5578–5593.

Zweng, M., Reagan, J., Antonov, J., Locarnini, R., Mishonov, A., and co-authors. 2013. Salinity. In S. Levitus and A. Mishonov, editors, *World Ocean Atlas 2013*, volume 2. NOAA Atlas NESDIS 74.

Table 1: Table of latitude boundaries for each of the estimates shown in Figs. 2 and 3. The Mediterranean and Baltic Seas are included in the ERA-Interim estimate at the relevant basin scales and in the latitude bands where they join the main Atlantic Ocean. BS refers to the Bering Strait and a star denotes that the latitudes shown are only approximate.

	ERA-Interim & ECCOv4			Dai and Trenberth (2003)		
	Atlantic	Pacific	Indian	Atlantic	Pacific	Indian
Fig. 2(b)	35°S-60°N	30°S-BS	>35°S	32°S-60°N	30°S-BS	>32°S
Fig. 2(a)	35°S-45°N	30°S-47°N		32°S-45°N	30°S-47°N	
Fig. 3	45°N-60°N	47°N-BS		45°N-60°N	47°N-BS	
Fig. 3	24°N-45°N	24°N-47°N	>8°S	24°N-45°N	24°N-47°N	>8°S
Fig. 3	16°S-24°N	17°S-24°N	20°S-8°S	16°S-24°N	16°S-24°N	20°S-8°S
Fig. 3	35°S-16°S	30°S-17°S	35°S-20°S	30°S-16°S	30°S-16°S	32°S-20°S
	Schanze *et al.* (2010)			Ganachaud and Wunsch (2003)		
	Atlantic	Pacific	Indian	Atlantic	Pacific	Indian
Fig. 2(b)	35°S-70°N*	35°S-BS	>35°S			>32°S
Fig. 2(a)	35°S-45°N	35°S-45°N		30°S-47°N	30°S-47°N	
Fig. 3	45°N-60°N	45°N-60°N				
Fig. 3	25°N-45°N	25°N-45°N	>5°S	24°N-47°N	24°N-47°N	>8°S
Fig. 3	15°S-25°N	15°S-25°N	25°S-5°S	19°S-24°N	17°S-24°N	20°S-8°S
Fig. 3	35°S-15°S	35°S-15°S	35°S-25°S	30°S-19°S	30°S-17°S	32°S-20°S
	Talley (2008)			Valdivieso *et al.* (2014)		
	Atlantic	Pacific	Indian	Atlantic	Pacific	Indian
Fig. 2(b)	32°S-59°N	30°S-BS	>32°S	32°S-70°N	32°S-BS	>32°S
Fig. 2(a)	32°S-45°N	30°S-47°N		32°S-47°N	32°S-47°N	
Fig. 3	45°N-59°N	47°N-BS		47°N-70°N	47°N-BS	
Fig. 3	24°N-45°N	24°N-47°N	>8°S	26.5°N-47°N	24°N-47°N	
Fig. 3	16°S-24°N		20°S-8°S	16°S-26.5°N	17°S-24°N	
Fig. 3	32°S-16°S		32°S-20°S	32°S-16°S	32°S-17°S	32°S-20°S

Table 2: Annual mean (1979-2014) area-averaged moisture budget residuals for the Atlantic and Pacific Oceans with $\bar{e}$, $\bar{p}$ and $\bar{e} - \bar{p}$ in mm/day.

	residual	$\bar{e}$	$\bar{p}$	$\bar{e} - \bar{p}$
Atlantic	0.08	4.01	2.69	1.32
Pacific	0.08	4.14	4.07	0.07

Table 3: Pearson correlations ($\widetilde{r}$) between annual means of ERA-Interim $\bar{e}$, $-\bar{p}$ and $\bar{e} - \bar{p}$ with div$\mathbf{Q}$ and standard deviations (σ, cm/yr) of $\bar{e}$, $-\bar{p}$, $\bar{e} - \bar{p}$ and div$\mathbf{Q}$.

	Atlantic		Pacific	
	$\widetilde{r}$	σ	$\widetilde{r}$	σ
$\bar{e}$	0.40	3.0	0.51	4.5
$-\bar{p}$	0.51	4.0	0.39	4.7
$\bar{e} - \bar{p}$	0.73	4.3	0.64	6.5
div$\mathbf{Q}$	1.0	3.0	1.0	2.1

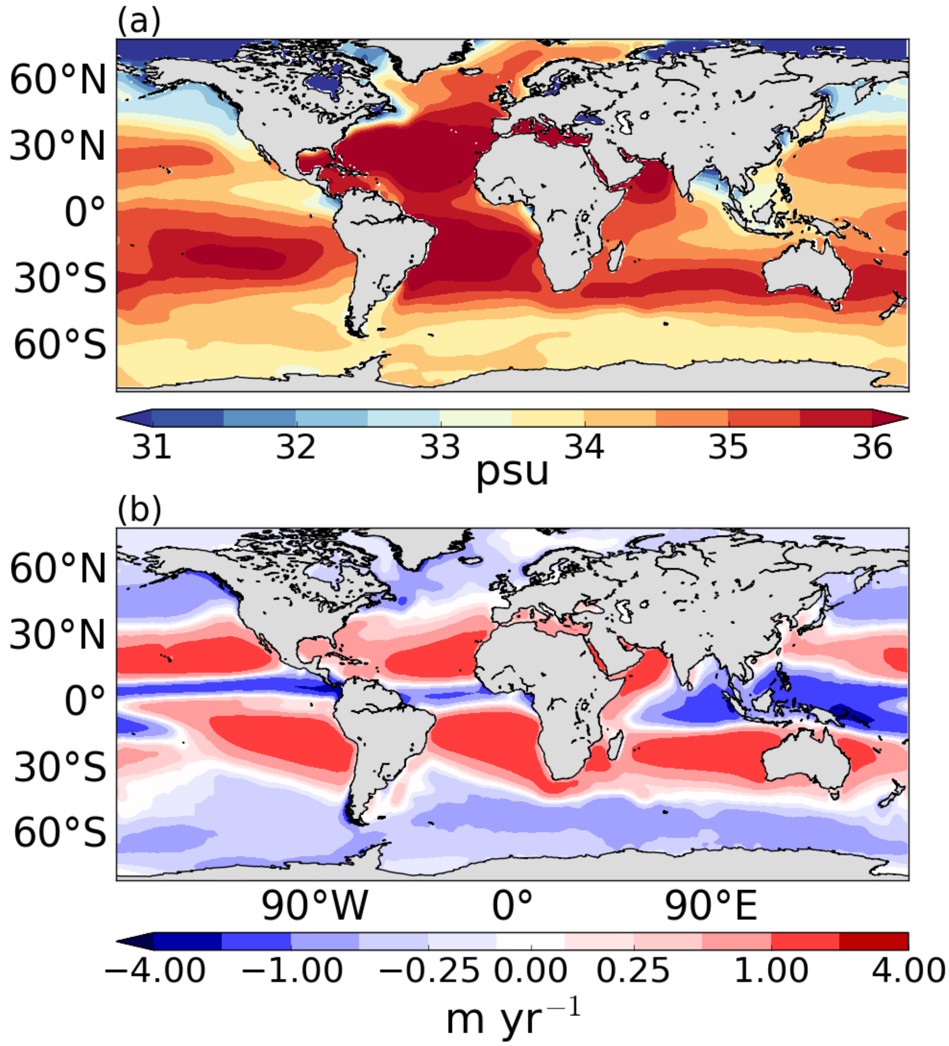

Figure 1: (a) Annual mean SSS (1955-2012) from the World Ocean Atlas (Zweng *et al.*, 2013) and (b) Annual mean (1979-2014) $e-p$ from ERA-Interim vertically integrated moisture flux divergence. Gaussian filter applied to smooth data.

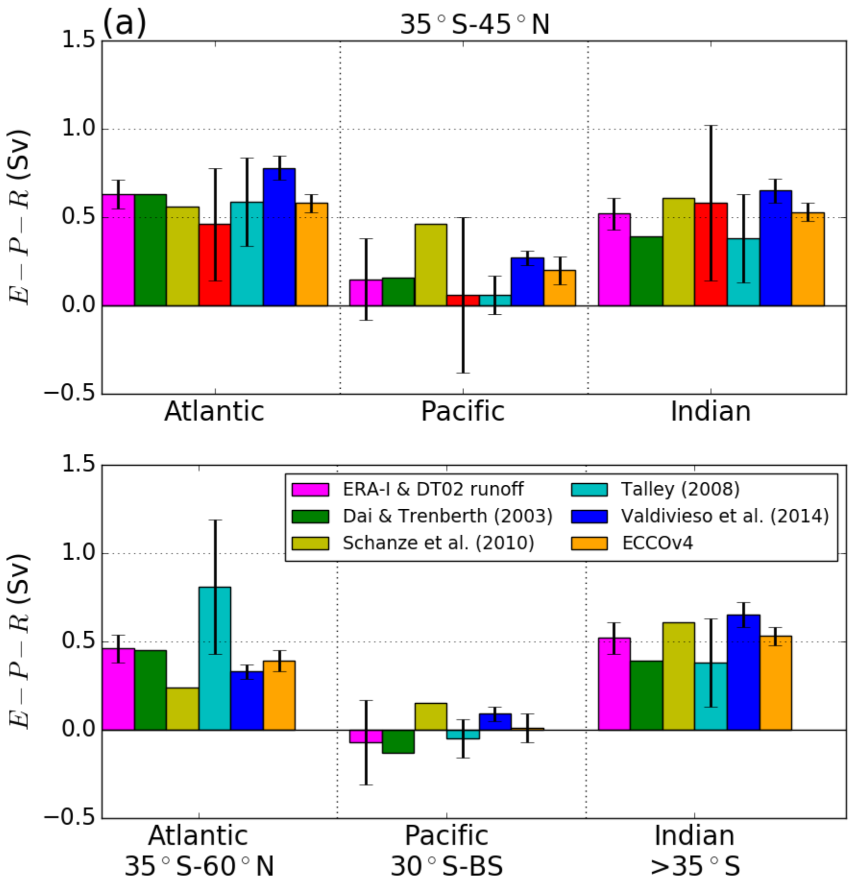

Figure 2: Basin-integrated net freshwater flux ($E - P - R$) for each ocean basin over different latitudinal extents: (a) approximately 35°S-45°N and (b) approximately 35°S-65°N. The latitude boundaries shown above each subfigure are approximate and do not apply to each estimate. Exact boundaries used in calculating each estimate are shown in Table 1. Estimates based on atmospheric data are shown first followed by the oceanographic estimates.

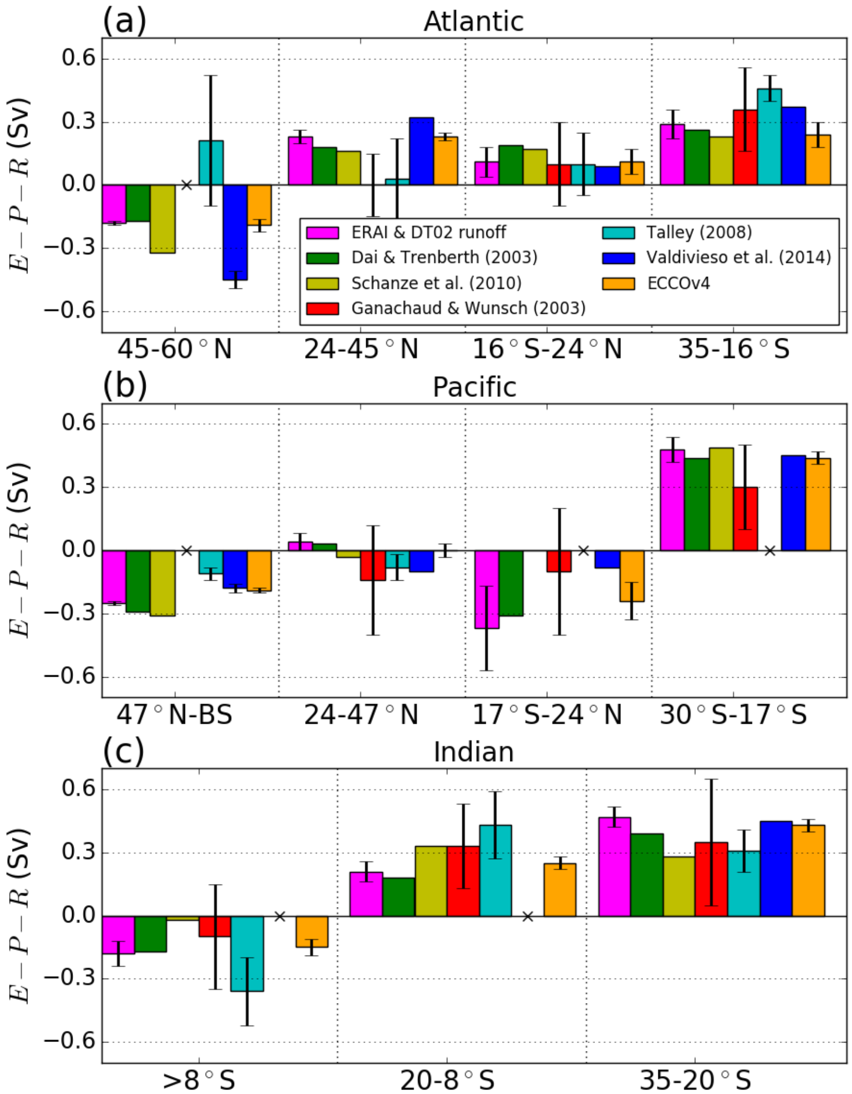

Figure 3: $E{-}P{-}R$ for latitude bands within the (a) Atlantic, (b) Pacific and (c) Indian oceans for the estimates described in section 3. Latitudes below each subfigure refer to those used to break up ERA-Interim. The exact boundaries used in calculating each estimate are shown in Table 1. Crosses denote that there is no estimate provided for a band, otherwise $E - P - R = 0$.

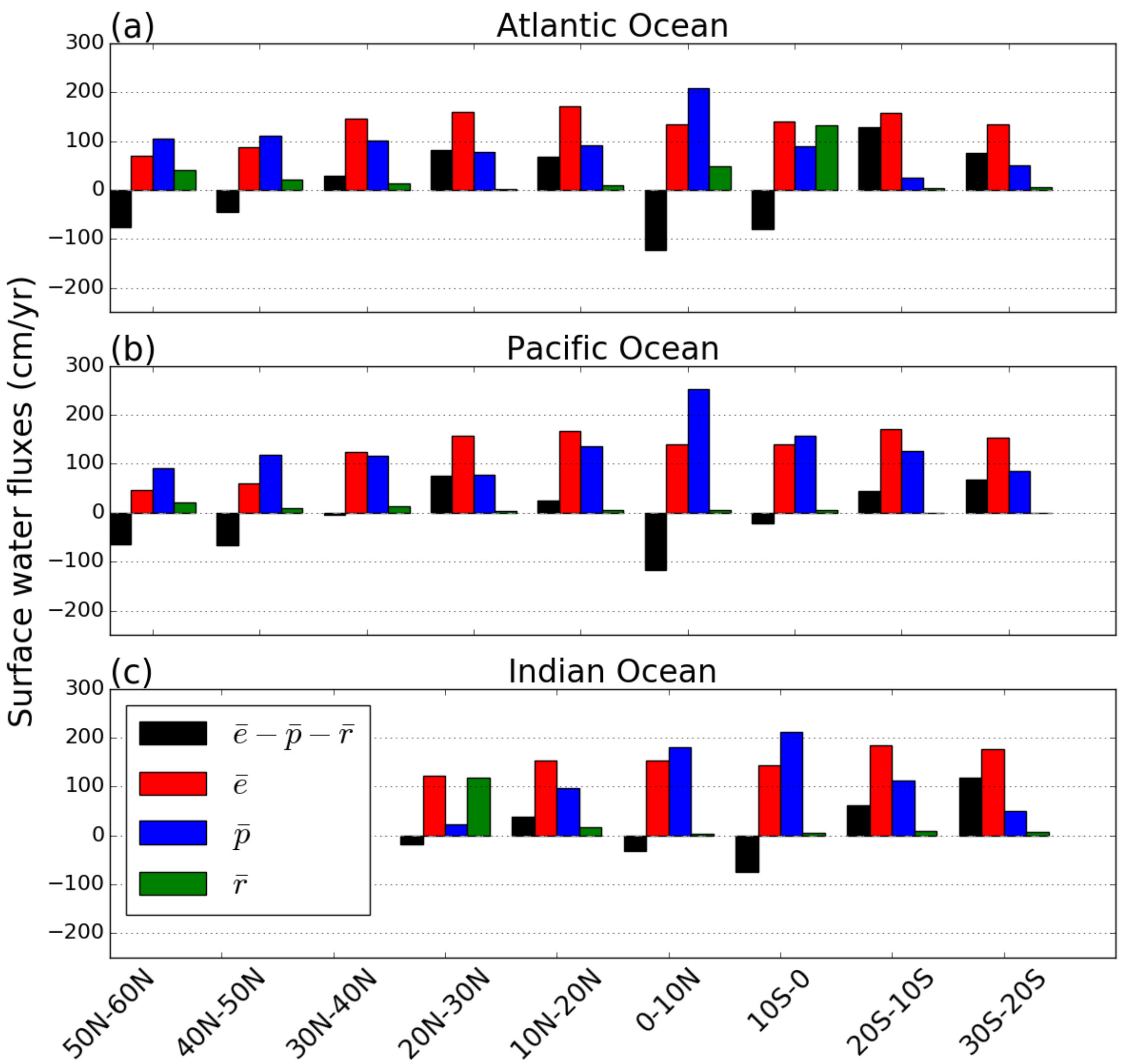

Figure 4: Annual mean area-averaged ERA-Interim (1979-2014) surface water fluxes in 10° latitude bands for the (a) Atlantic, (b) Pacific and (c) Indian oceans with Dai and Trenberth (2002) runoff divided into the same 10° latitude bands.

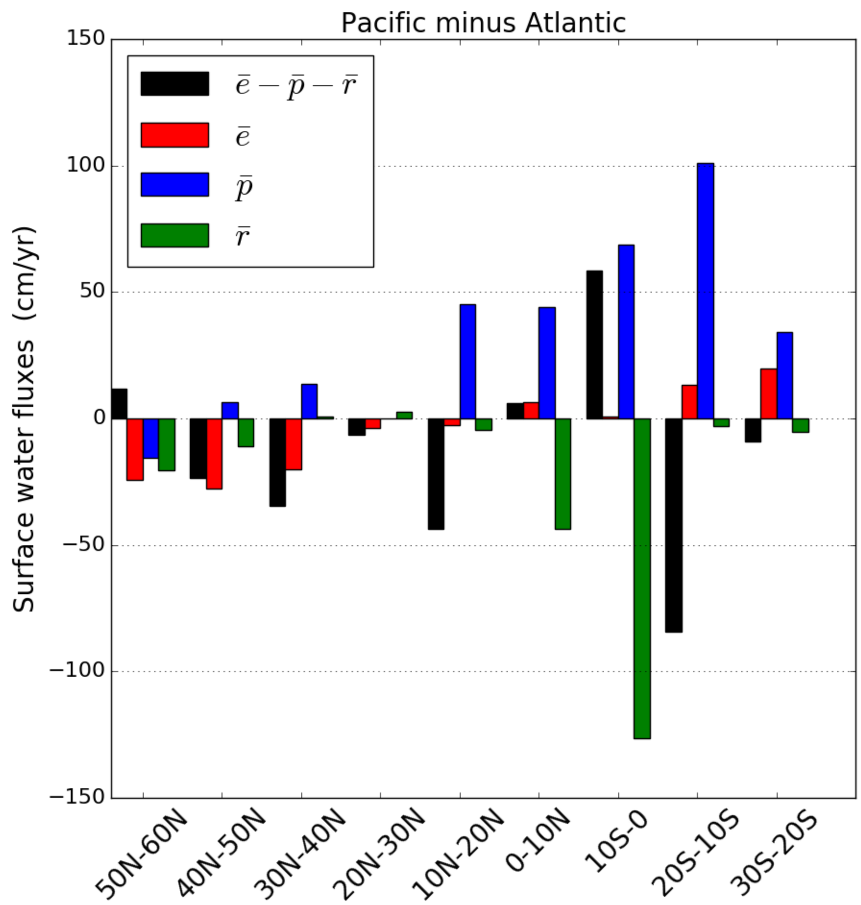

Figure 5: Differences between area-averaged annual mean ERA-Interim (1979-2014) Pacific and Atlantic surface water fluxes in 10° latitude bands scaled by area with Dai and Trenberth (2002) runoff divided into the same 10° latitude bands.

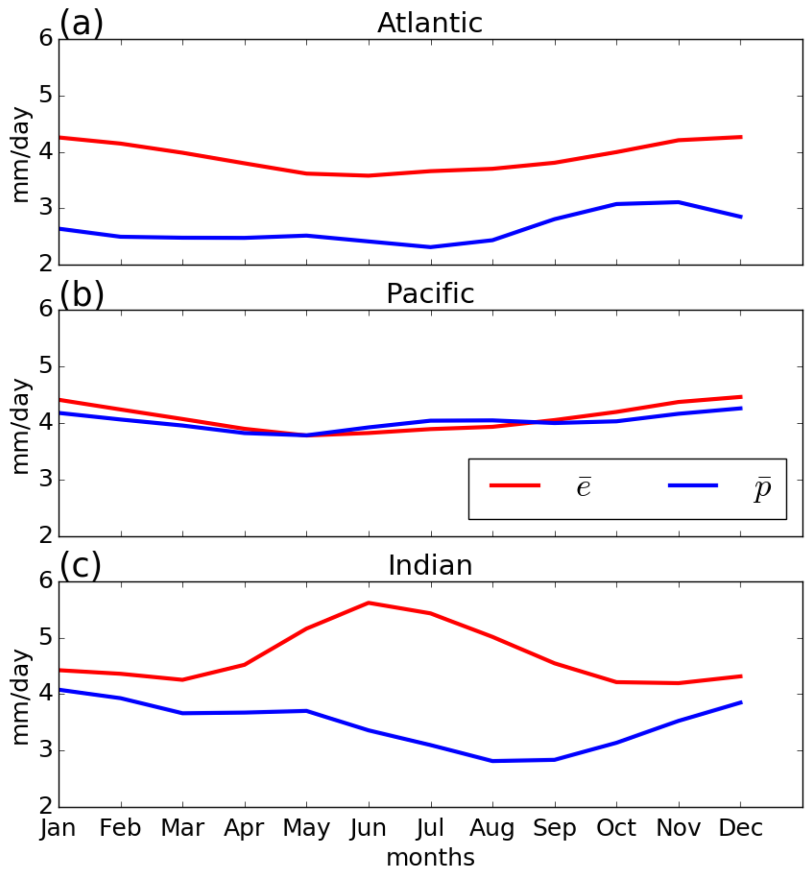

Figure 6: Climatological monthly means (1979-2014) of ERA-Interim $\bar{e}$ and $\bar{p}$ for the (a) Atlantic (35°S-60°N), (b) Pacific (30°S-Bering Strait) and (c) Indian (>35°S) Oceans at basin scale (first row of ERA-Interim columns in Table 1).

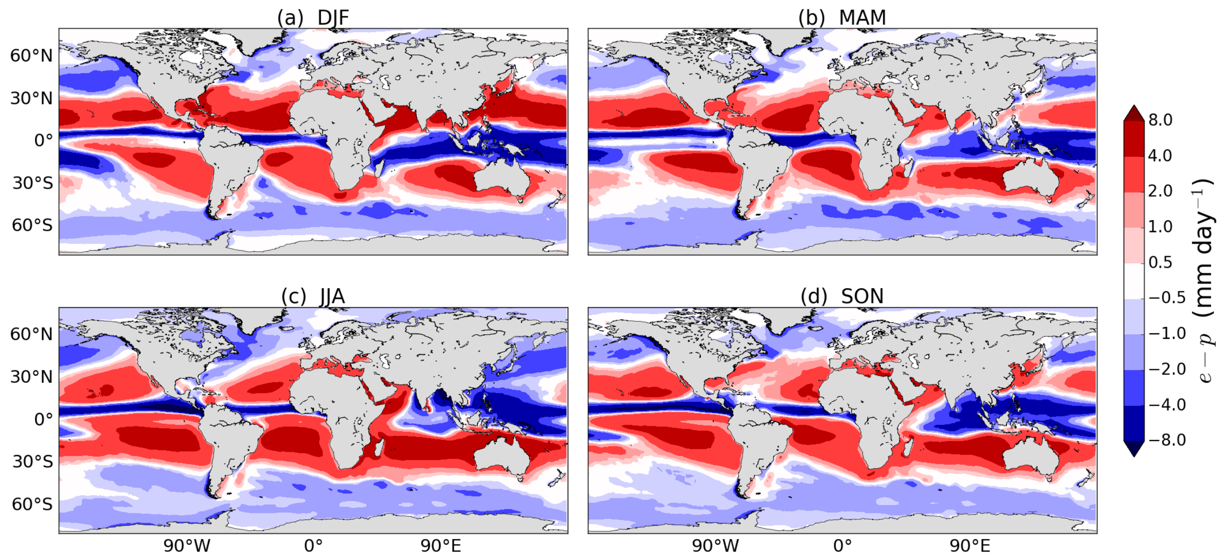

Figure 7: Climatological seasonal mean ERA-Interim $e-p$ from accumulated surface forecasts 1980-2014 for (a) December-January-February (DJF), (b) March-April-May (MAM), (c) June-July-August (JJA) and (d) September-October-November (SON).

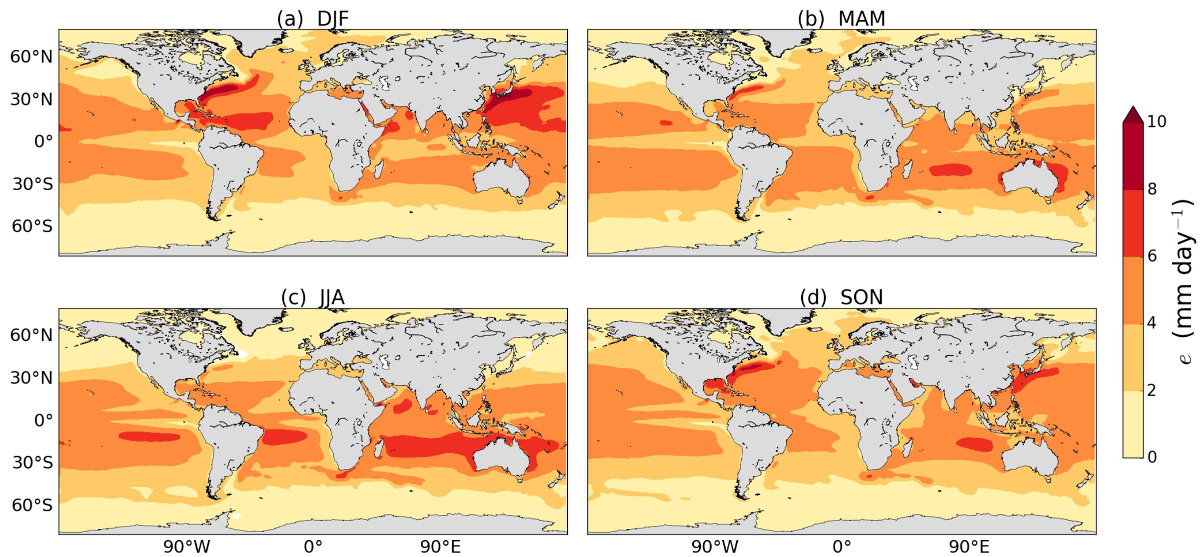

Figure 8: Climatological seasonal mean ERA-Interim evaporation 1980-2014 for (a) DJF, (b) MAM, (c) JJA and (d) SON.

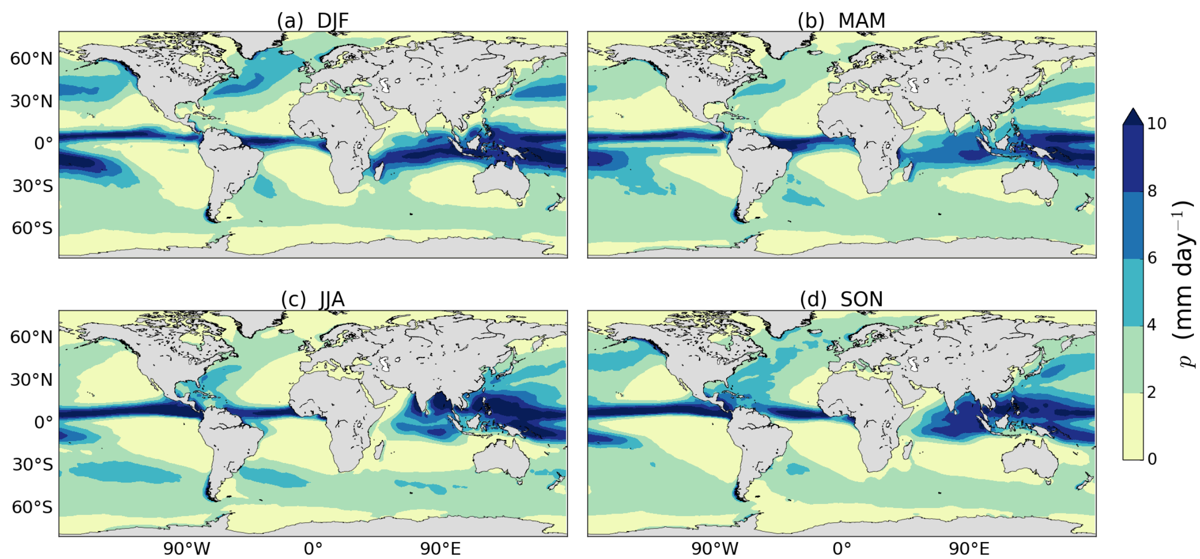

Figure 9: Climatological seasonal mean ERA-Interim precipitation 1980-2014 for (a) DJF, (b) MAM, (c) JJA and (d) SON.

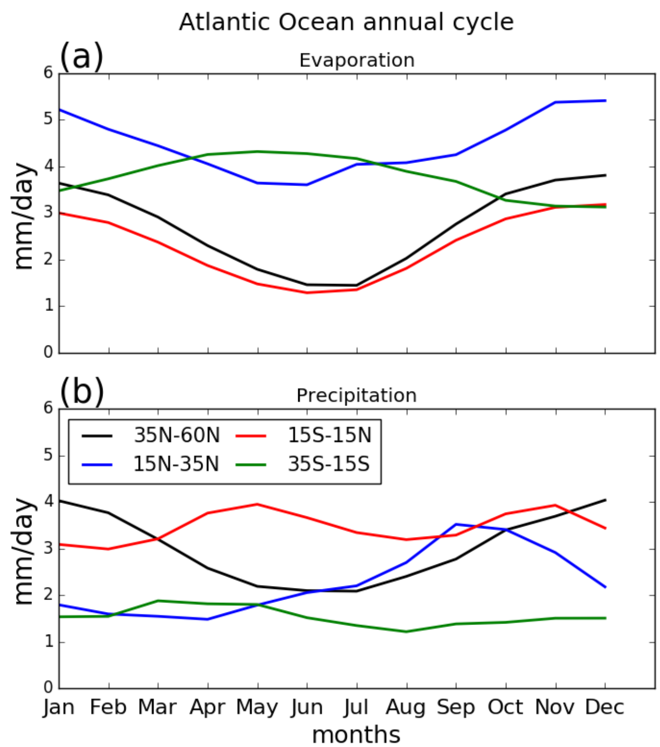

Figure 10: Climatological monthly means of ERA-Interim (1979-2014) Atlantic Ocean area-averaged (a) evaporation and (b) precipitation in latitude bands representing the tropics, subtropics and northern hemisphere extratropics.

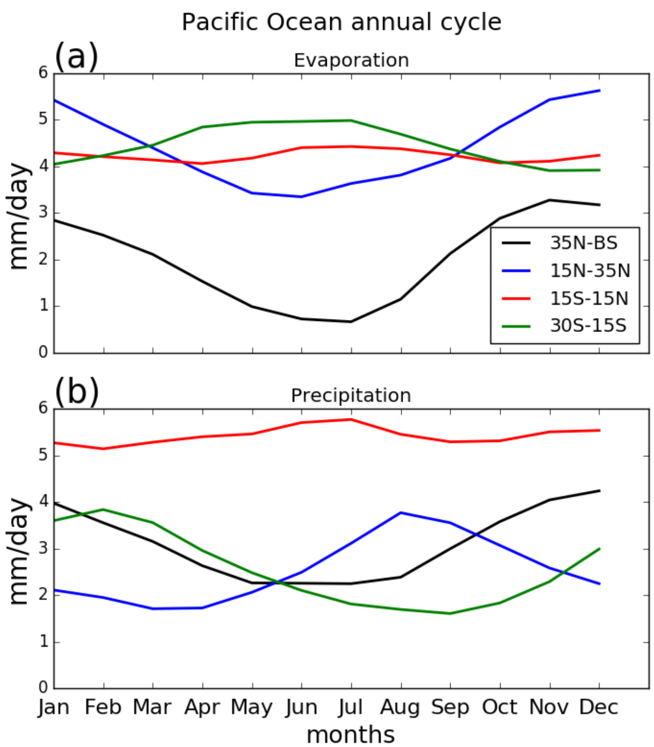

Figure 11: Climatological monthly means of ERA-Interim (1979-2014) of Pacific Ocean area-averaged (a) evaporation and (b) precipitation in latitude bands representing the tropics, subtropics and northern hemisphere extratropics.

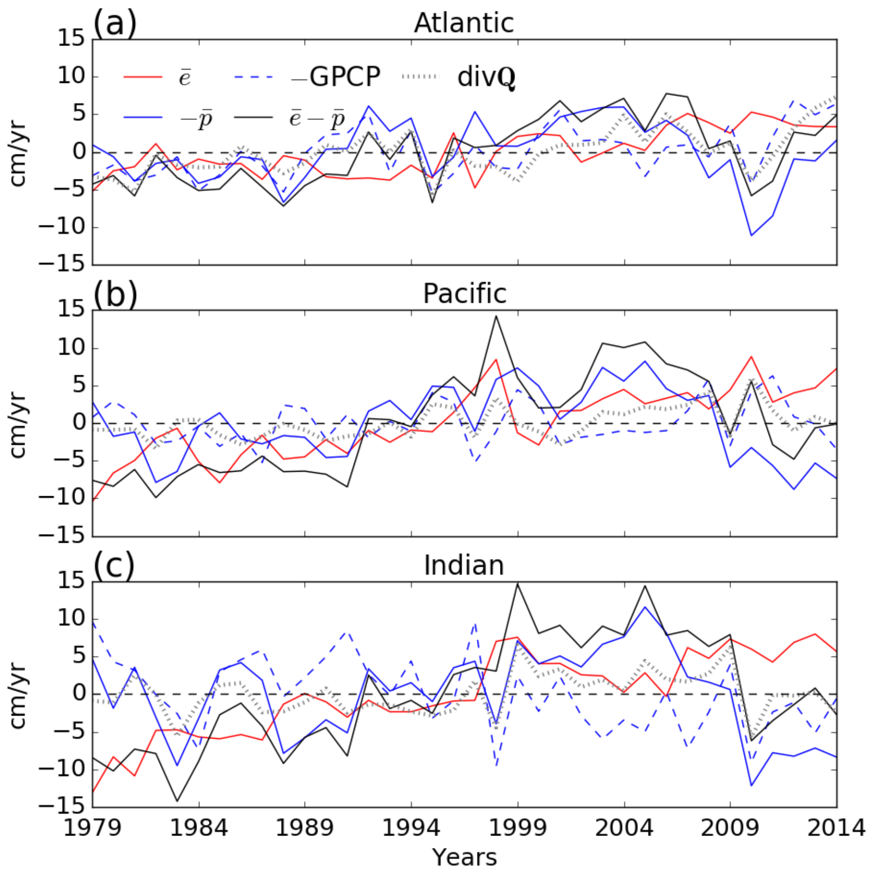

Figure 12: Yearly anomalies from the 1979-2014 area-averaged annual mean ERA-Interim $\bar{e}$, $-\bar{p}$, $\bar{e}-\bar{p}$, div$\mathbf{Q}$ and -GPCP for the (a) Atlantic, (b) Pacific and (c) Indian oceans at basin scale (first row of ERA-Interim columns in Table 1).